

D4.2 – PARAMETRIC STUDY ON SLAT TRACK NOISE GENERATION AND MITIGATION AND SELECTION OF BEST LOW-NOISE SLAT TRACK DESIGNS

Document authors	Evelien van Bokhorst (NLR)
Document contributors	Johan Kok (NLR), Marthijn Tuinstra (NLR)

Abstract

High lift system leading edge noise, slat track noise generation and reduction, experimental and numerical investigations

Information Table

Project information	
PROJECT ID	860538
PROJECT FULL TITLE	INnoVative dEsign of iNstalled airframe componenTs for aircraft nOise Reduction
PROJECT ACRONYM	INVENTOR
FUNDING SCHEME	RIA -Research and Innovation Action
START DATE OF THE PROJECT	01-05-2020
DURATION	48 months
CALL IDENTIFIER	H2020-MG-2018-2019-2020


Deliverable information	
DELIVERABLE No AND TITLE	D4.2
TYPE OF DELIVERABLE	Report
DISSEMINATION LEVEL	Public
BENEFICIARY NUMBER AND NAME	9 - STICHTING NATIONAAL LUCHT- EN RUIMTEVAARTLABORATORIUM (NLR)
AUTHORS	Evelien van Bokhorst (NLR)
CONTRIBUTORS	Johan Kok (NLR), Marthijn Tuinstra (NLR)
WORK PACKAGE No	4
WORK PACKAGE LEADER WP LEADER VALIDATION DATE	Michael Pott-Pollenske (DLR) October 26 th 2022
COORDINATOR VALIDATION DATE	October 28 th 2022
Coordinator signature	

Table of Contents

Abstract	1
Information Table.....	1
1 Introduction	3
2 Slat track design	4
2.1 Variations on Dassault baseline slat track	4
2.1.1 Selection of important slat track design parameters.....	4
2.1.2 Mean flow computations on simplified slat track	4
2.1.3 Final design of slat tracks	6
2.2 Variations on Airbus baseline slat track	8
3 Experimental set-up	8
3.1 Wind tunnel model	8
3.2 Acoustic beamforming	9
3.3 Set-up in the AWT.....	9
3.4 Data processing techniques.....	10
5. Repeat for different frequencies to obtain power integrated spectra.....	11
3.5 Test matrix	12
4 Results and discussion.....	13
4.1 Static pressure measurements.....	13
4.2 Array measurements	13
4.2.1 Beamform maps	13
4.2.2 Power integrated spectra, variations on Dassault baseline	14
4.2.3 Power integrated spectra, variations on Airbus baseline	17
4.2.4 Velocity scaling of noise levels	17
5 Conclusion	19
6 Bibliography	20

1 Introduction

The INVENTOR project aims to better understand the physics of noise generated by landing gears and high lift devices. This report, Deliverable 4.2, is written as part of Task 4.2, which is concerned with a preliminary assessment of low-noise slat tracks.

The slat track is the mechanism which connects the slat with the main wing and has shown to be a dominant noise source in previous studies (Dobrzynski, et al., 1998; Dobrzynski, et al., 2008; Piet, et al., 2012; Murayama, et al., 2015; Murayama, et al., 2016; Wang, et al., 2013). The main contribution to slat track noise originates from the cavity where the slat track is retracted from. When the cavity is sealed off significant noise reductions are found (Dobrzynski, et al., 2008; Murayama, et al., 2016). The effect of the door panel and rail geometry on noise generation have been studied experimentally and computationally in (Murayama, et al., 2015; Murayama, et al., 2016). When the panel is omitted and the rail cross section is rectangular instead of an I-shape geometry, reductions in the order of a few dB were found. In the current investigation the previous work is extended with the following approach. First, RANS simulations are carried out on a simplified slat track design to identify possible noise generation mechanisms. Based on the results from the simulations, low-noise slat tracks were designed and manufactured. Then both, the baseline and low-noise slat tracks, were tested in the aeroacoustic wind tunnel (AWT) at NLR Marknesse.

The report is structured as followed. In Chapter 2 is focussed on the design of low-noise slat tracks by first discussing the results of the RANS simulations from which the low-noise designs were derived. In Chapter 3 the experimental set-up and measurement techniques used in the experiment in the aeroacoustic wind tunnel (AWT) at NLR Marknesse are described. The results are given as discussed in Chapter 4 and the report ends with the conclusions.

2 Slat track design

The study on slat track noise covers two generally different track design as used for commercial airliners on the one hand and business jets on the other hand. Both types of tracks were investigated experimentally while only the business jet type slat tracks were also shape optimized on basis of numerical flow simulations.

2.1 Variations on business type slat track

2.1.1 Selection of important slat track design parameters

From previous investigations the details of the slat track which contributed most to slat track noise were identified. As also stated in the introduction the main parameters which had an influence on the slat track noise levels were:

- Coverage of cavities: covering of the space between the main wing and the slat track showed to have the largest effect on the slat track noise levels. The effect of this geometrical feature is also part of DAV's Background DGT 176808.
- Size of panel: the panel closes the cavity on the main wing when the slat is not deployed. When the panel is not present the noise level is decreased.
- Alignment of slat track with the flow: when the slat tracks were aligned with the flow this led to a decrease in slat track noise.
- Shape of the slat bracket: when the cross section of the slat bracket was filled the slat track noise reduced. Modification of the side sections of the slat track to get an aerodynamical shape to reduce noise is part of DAV's Background DGT 176808.

In the current study the focus will be on these details of the slat track. To better understand the exact noise generation mechanisms mean flow computations were carried out.

2.1.2 Mean flow computations on simplified slat track

For the RANS computations (with EARSM turbulence model) a simplified slat track is used as shown in Figure 1. For this slat track geometry there was no leading-edge opening, since from previous studies it was already known that this is a dominating noise mechanism for slat track noise. Instead the focus here is on other mechanisms. The slat track has been added to a swept high lift system with slat featuring a retracted chord length of $c = 300$ mm and a sweep angle $\Lambda = 30^\circ$ (see section 3.3). The freestream velocity was 71 m/s with a chord Reynolds number, Re_c , of 1.46×10^6 , and an angle of attack of $\alpha_s = 15.72^\circ$. In deliverable D2.3, the angle of attack was optimized to a value of $\alpha_o = 18^\circ$ for the 2-element wing, but using a 2D computation of the wing without sweep and with a side slip angle of 30° . In order to obtain essentially the same flow in the 2D plane normal to the leading edge, the angle of attack was determined by the relation $\tan \alpha_s = \cos \Lambda \cdot \tan \alpha_o$ for the current 3D computations of the swept wing. (It was verified that the same pressure distribution was obtained in this way for the case without slat track.) The spanwise extent was 100 mm ($= c/3$) and periodic conditions were applied. An overset multi-block grid with overlapping grids for wing, slat, and slat track was created with 6.5 million grid cells (wing: 4.0 million, slat: 1.8 million, slat track: 0.7 million).

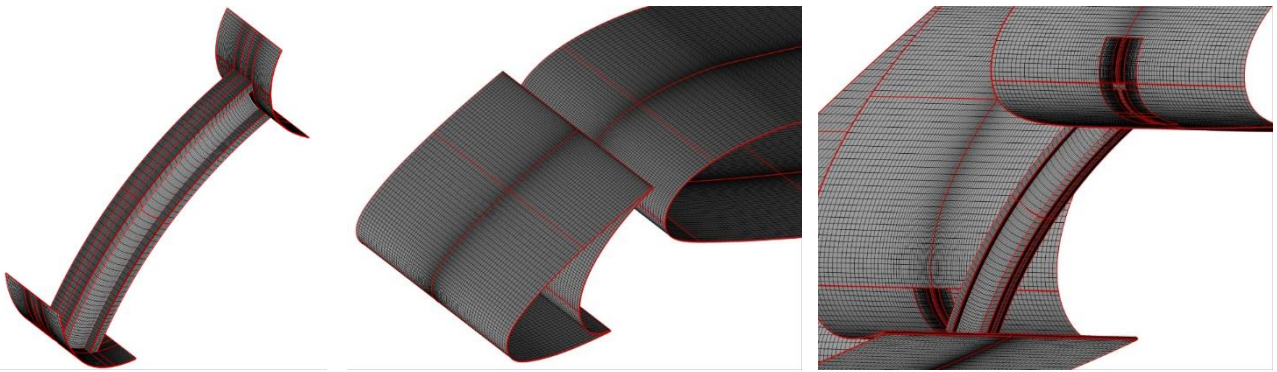


Figure 1: Simplified slat track geometry (left). Slat and wing (middle). Slat track connected to wing and slat (right). In black the surface grid lines are shown and in red the edges of the multi-block grid.

The flow in the vicinity of the slat track is shown in Figure 2 in terms of vorticity magnitude and turbulent kinetic energy. Due to the sweep angle and the angle of attack, the flow comes from the lower left side and separates at the upper left and lower right corners of the slat track. Two areas can be distinguished: over roughly the first half of the slat track (within the slat cove), the flow is mainly going sideways (span-wise direction), leading to a separated flow region to the right of the slat track. Over the second half of the slat track (near the wing), there is a strong flow going upwards, being sucked through the gap between the slat and the wing. The separated shear layers on the left and right sides are transported upwards by this strong flow and roll up into counter-rotating vortices. High levels of turbulent kinetic energy are found in this area, in particular in the shear flow between the vortices.

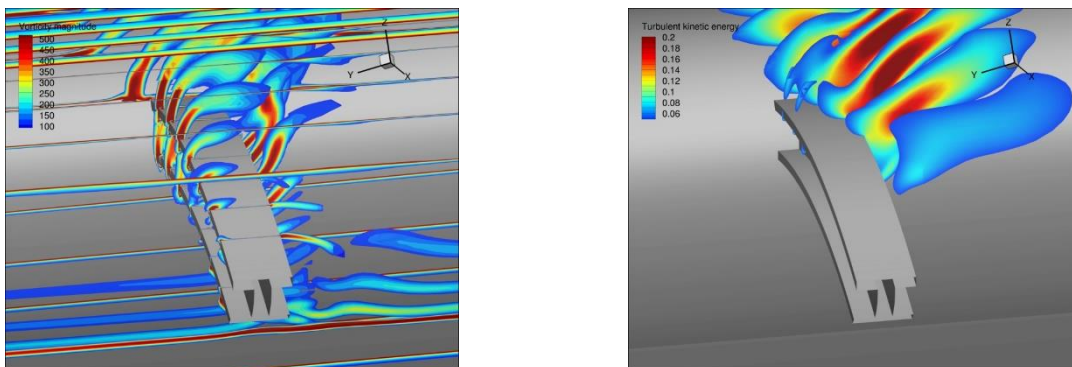


Figure 2: Iso-contour plot of vorticity magnitude ($\Omega c/u_\infty$, left) and turbulent kinetic energy (k/u_∞^2 , right) in slices normal to the cord-wise direction.

To support the design of low-noise slat tracks, in particular the tilted fairing (see below), the direction of the undisturbed flow (without slat track) at the location of the slat track has also been computed for the 2D swept wing, which already illustrates the two distinct flow regions (Figure 3).

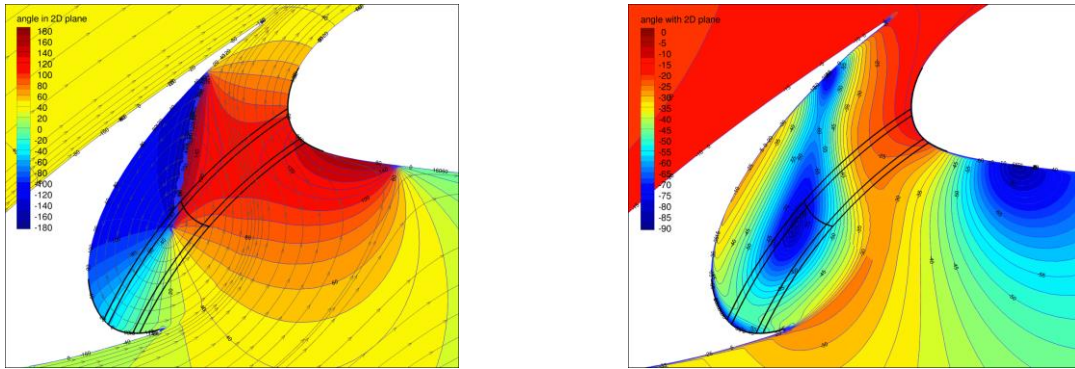


Figure 3: Direction of undisturbed flow in slat track region. Left: in-plane streamlines and iso-contours of local angle of attack (flow angle in 2D plane). Right: iso-contours of local angle of side slip (flow angle with 2D plane).

2.1.3 Final design of slat tracks

First several baseline slat tracks are defined to quantify the effect of different geometric parameters which were also tested in previous investigations. In Figure 4 the baseline slat tracks are shown.



Figure 4: Baseline slat tracks with the differences between them indicated.

For the low-noise slat tracks the leading edge cavity is omitted since previous studies have shown that this is the dominating slat track noise source. By omitting the cavity the focus is on the smaller details of the slat track. The first set of low-noise slat tracks has a fairing around the slat track rail which will avoid separation and consequently reduce the noise.



Figure 5: Low-noise slat track designs with upstream and or downstream fairing.

The next set of low-noise slat tracks are designed by using the RANS computations. From the RANS computations it follows that there are two noise generating mechanisms. The first and dominating mechanism is the separated flow located close to the connection between the slat track and main wing. As shown in Figure 3 the flow is coming from the bottom of the slat track and then separates at the top. To reduce the noise created by this source a tilted fairing was designed where the tilt angle is the same as the one found from the RANS simulations. The second noise generating mechanism is caused by the cross-flow separating in a region close to the connection between the slat and slat track. To reduce the noise created by this source, an open slat track design is designed such that the cross-flow will not be obstructed by the slat track. In Figure 6 the low-noise slat track designs are shown.

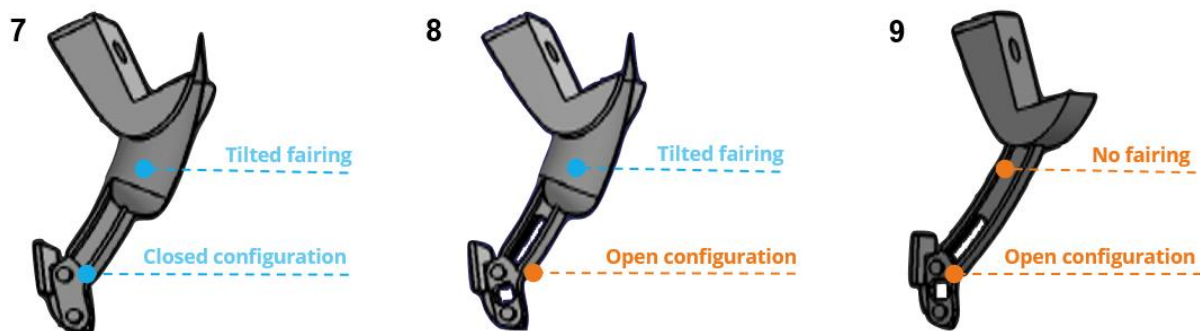


Figure 6: Low-noise slat track designs with a tilted fairing and or opening.

Finally, in Figure 7 the flow aligned slat track is shown.



Figure 7: Design of flow-aligned slat track.

All slat tracks were 3D printed.

2.2 Variations on the SMR commercial airliner Airbus slat track

In Figure 8 different variations on the Airbus baseline slat track are shown. The main focus is on the shape of the slat track bracket where small differences in thickness and size are applied.



Figure 8: Variations on slat track provided by DLR and Airbus.

3 Experimental set-up

3.1 Wind tunnel model

The DLR F16 model was originally designed for tests in DLR's AWB with 0° sweep and a span of 800 mm. In a past ONERA-DLR cooperation named SWAHILI it has been extended to a span of 1400 mm and a 30° sweep for tests in ONERA's F2 (Manoha, et al., 2018). For the current tests the model with sweep will be used. The original 3-element model (slat,wing,flap) was modified in the current project to create a 2-element model where the flap is replaced by a trailing edge (Figure 9). The angle of attack of the main wing and vertical position of the trailing edge were determined by an optimization procedure for which the details can be found in the report of deliverable 2.3¹.

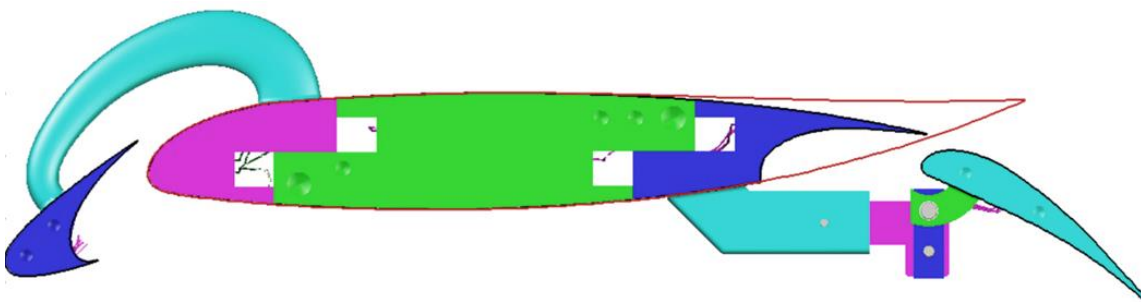


Figure 9: Cross-section of original DLR's F16 model with slat, wing and flap. Modification is shown with the red outline such that a 2 element model can be created (slat and wing).

¹ van Bokhorst E., Terracol M., Fleury V. REPORT ON Specifications for PRELIMINARY experimental (AWT/NLR) and numerical studies on slat track noise in WP4

3.2 Acoustic beamforming

To localize and quantify acoustic sources from the slat track acoustic array measurements were carried out. An acoustic array consists of a number of microphones which are distributed in such a way that sources in a large frequency range can be measured. With the signals and time delays measured for each microphone an acoustic source map is constructed by applying a beamforming algorithm. For conventional beamforming the auto powers in the source map are determined with:

$$A = \frac{\mathbf{g}^* \mathbf{C} \mathbf{g}}{\|\mathbf{g}\|^4}$$

where \mathbf{C} is the cross-power matrix, and \mathbf{g} the steering function. The sound source is described as a monopole in a uniform flow in which case the steering function writes:

$$g_{mono} = \frac{-e^{2\pi i f \Delta t_e(x_n, \xi_n)}}{4\pi \sqrt{(M \cdot (x_n - \xi_n))^2 + \beta^2 \|x_n - \xi_n\|}} = \frac{-e^{2\pi i f \Delta t_e(x_n, \xi_n)}}{4\pi R}$$

where f is the frequency, $\Delta t_e(x_n, \xi_n)$ the time delay for microphone x_n and grid point ξ_n , M the Mach number and $\beta = (1 - M^2)$.

3.3 Set-up in the AWT

Experiments are carried out in the Aeroacoustic Wind Tunnel (AWT) at NLR Marknesse. The wind tunnel can be operated with both a closed test section and open-jet configuration. For the current experiment the open-jet configuration with a 0.8mx0.6m nozzle has been used. The anechoic chamber, with a volume of 11x7x5m (lxbxh) has a cut-off frequency of 315Hz. A 64 channel array (PCB free-field microphones) and 5 free-field microphones (M51) were connected to a HDR viper system to acquire data with 102.4kHz for 30 seconds. The array was placed on a traverse system such that the array could be traversed in the x and z direction. In Figure 10 a schematic and picture of the set-up are shown. Next to the microphones, static pressure ports were embedded in the wing and slat. In this test the pressure distribution in the slat region is important which can be resolved by 13 pressure ports installed on the slat. The coordinate system is also shown in Figure 10 where the origin is chosen in the middle of the slat track.

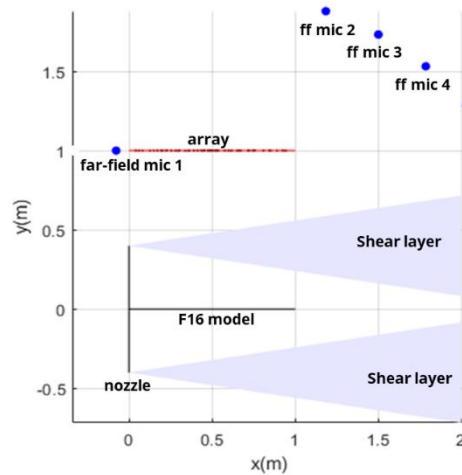


Figure 10: Experimental set-up with the microphone set-up (left) and picture of the set-up (right).

3.4 Data processing techniques

To obtain source maps and power integrated spectra conventional beamforming techniques are used. For the power integrated spectra the technique described in (Sijtsma & Stoker, 2004) is followed and consists of the following steps:

1. Create grid with slat track noise source in the middle.
2. Integrate auto-powers, A , obtained with conventional beamforming on H grid points.
3. Integrate auto-powers of simulated point source in the middle of scan grid with $P_s=1$.
4. Obtain source power, P , estimate with

$$P = \frac{\sum_{h=1}^H A_h}{\sum_{h=1}^H A_{s,h}} \times P_s$$

5. Repeat for different frequencies to obtain power integrated spectra.

Next to conventional array measurements, tomographic beamforming was applied on a selected number of points. This method allows the reconstruction and deconvolution of three dimensional source fields (Tuinstra & van der Meulen, 2019). To apply this method the array was traversed to different locations such that source maps from different view angles were obtained.

A system of linear algebraic equations was defined using the array responses and relating them by a physical model to the sources found in the reconstruction domain. This system of equations is then iteratively solved using an existing tomographic algorithm (RBI-EMML) to obtain the source field which matches most closely the information provided by the array measurements at different locations.

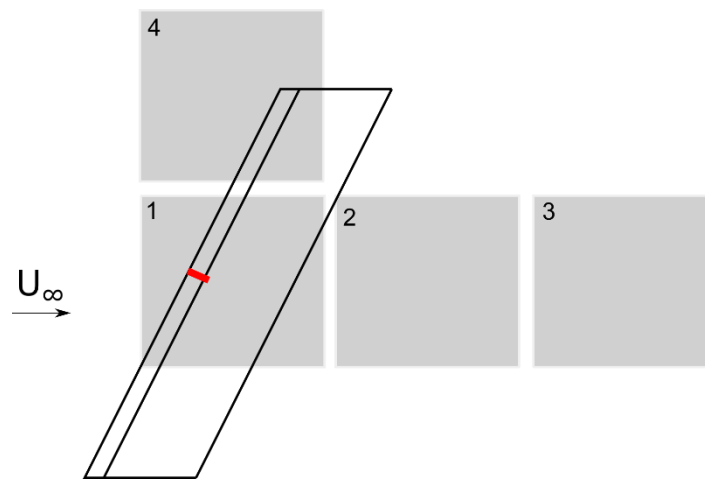


Figure 11: Set-up for tomographic beamforming measurements. In red the location of the slat track is denoted. The grey squares represent the different locations of the array. For clarity the array positions are shown without overlap.

In the results section the business jet slat track data are represented in terms of SPL deltas relative to slat track 2 (Figure 5). Δ is defined as:

$$\Delta = SPL - SPL_{slat\ track\ 2}$$

Slat track 2 does not have a leading opening, does have a door panel and has an I-shaped cross section. In case of the commercial airliner platform the slat track no. 11 serves as reference for the level difference computation.

3.5 Test matrix

INVENTOR: Slat track noise investigation in the AWT			
Measurement techniques		#	Slat track geometry
Array measurements		0	No slat track
Directivity measurements		1	Baseline DaV 1
Static pressure measurements		2	Baseline DaV 2
Optional: flow visualizations with tufts		3	Baseline DaV 3
		4	Low noise DaV 1
Acoustic measurement parameters		5	Low noise DaV 2
Sample frequency (kHz)	102.4	6	Low noise DaV 3
Measurement time (s)	30	7	Low noise NLR 1
Total test cases	50	8	Low noise NLR 2
Array aperture, m	0.95	9	Low noise NLR 3
Array distance, m	1	10	Low noise NLR 4
Number of array microphones	64	11	Low noise DLR black
		12	Low noise DLR gray
Velocity		13	Low noise DLR red
$U_{inf} = 71\text{m/s}$		14	Low noise DLR yellow

The following measurements were performed:

- An alpha-sweep to find the optimal angle of attack for which the slat pressure distribution matches a reference measurement, this was found at 21.3°
- Measurements with a known reference source (speaker emitting white noise or 3kHz tone) as system checks
- Noise measurements without slat track, for varying velocity (21, 31,41,51,61 and 71m/s)
- Noise measurements for slat track 1, for varying velocity (21, 31,41,51,61 and 71m/s)
- Noise measurements for slat track 2, for varying velocity (21, 31,41,51,61 and 71m/s)
- Noise measurements for slat track 3, for varying velocity (21, 31,41,51,61 and 71m/s)
- Noise measurements for slat track 4, for varying velocity (21, 31,41,51,61 and 71m/s)
- Noise measurements for slat track 5, for varying velocity (21, 31,41,51,61 and 71m/s)
- Noise measurements for slat track 6, for varying velocity (21, 31,41,51,61 and 71m/s)
- Noise measurements for slat track 7, for varying velocity (21, 31,41,51,61 and 71m/s)
- Noise measurements for slat track 8, for varying velocity (21, 31,41,51,61 and 71m/s)
- Noise measurements for slat track 9, for varying velocity (21, 31,41,51,61 and 71m/s)
- Noise measurements for slat track 10, for varying velocity (21, 31,41,51,61 and 71m/s)
- Noise measurements for slat track 11, for varying velocity (21, 31,41,51,61 and 71m/s)
- Noise measurements for slat track 12, for varying velocity (21, 31,41,51,61 and 71m/s)
- Noise measurements for slat track 13, for varying velocity (21, 31,41,51,61 and 71m/s)
- Noise measurements for slat track 14, for varying velocity (21, 31,41,51,61 and 71m/s)
- Noise measurements for slat track 1, at freestream velocity 71m/s for different array positions ($\Delta x=0, 0.35$ and 0.7m ; $\Delta z=0,0.34,0.68\text{m}$)
- Noise measurements for slat track 7, at freestream velocity 71m/s for different array positions ($\Delta x=0, 0.35$ and 0.7m ; $\Delta z=0,0.34,0.68\text{m}$)

4 Results and discussion

4.1 Static pressure measurements

In Figure 12 the static pressure distributions are shown for different angles of attack together with the target pressure distribution. From the free-field simulations an angle of attack of 18 degrees was predicted which was taken as a starting point. In the experimental set-up close resemblance with the target distribution was obtained at $\alpha=21.3^\circ$. This angle of attack was set for the rest of the experiment.

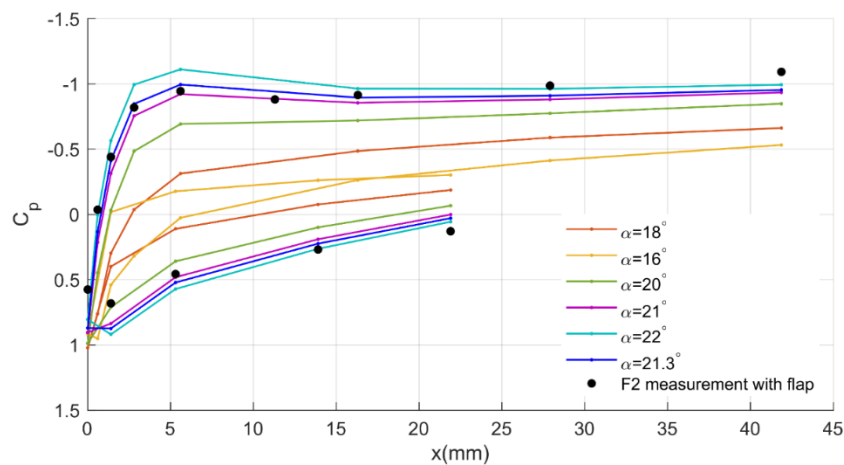


Figure 12: Static pressure distribution for different angles of attack compared to pressure distribution of previous measurements.

4.2 Array measurements

4.2.1 Beamform maps

Next the results of the acoustic array measurements are discussed. First it was checked if slat track noise was dominant. In Figure 13 the source map without and with slat track are shown at a frequency of 4kHz, 6kHz and 10kHz. For 4kHz sources are detected that coincide with the slat bracket locations (see Figure 10, left), used to attach the slat to the main wing element. At 6kHz the noise originating from the bracket is still visible, but the slat track noise is appearing stronger. At 10kHz only the slat track is found in the beamforming map. The tomographic source reconstruction (Tuinstra & van der Meulen, 2019) for slat track 1 is shown in Figure 14 and confirm the observations from the 2D image maps. Inspection of beamforming maps for different frequencies showed that from approximately 7.5kHz and above the slat track noise is dominant in the beamforming map. Below 7.5kHz bracket noise is contaminating the power integrated noise measurements, hampering interpretation.

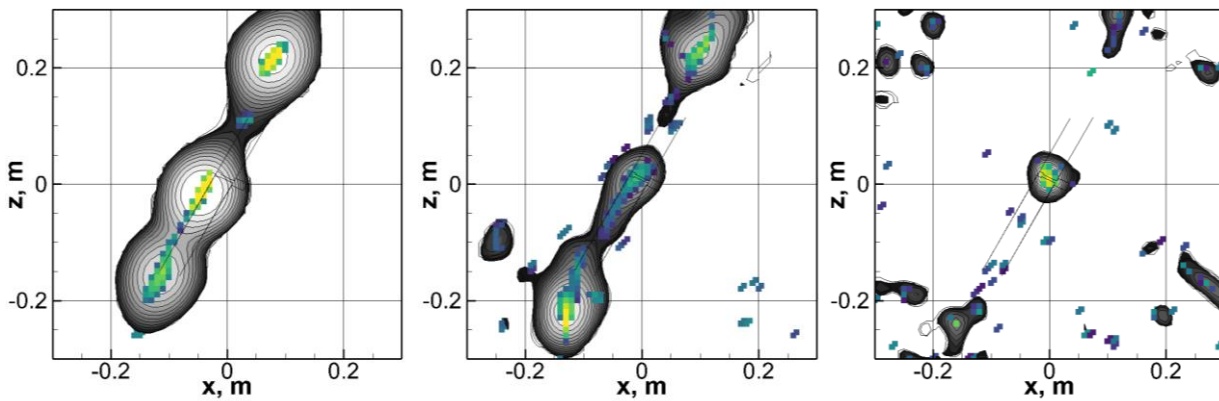


Figure 13: Beamform maps at 4kHz (left), 6kHz (centre) and 10kHz (right) with slat track 1 installed. The dB range is 12dB. Colour contours depict the deconvoluted source field and grey contours the conventional beamforming maps.



Figure 14 Tomograms for slat track 1; 4kHz (left); 6kHz (centre) and 10kHz (right)

4.2.2 Power integrated spectra, variations on Dassault baseline

In Figure 12 the relative levels of the integrated power spectra for the baseline slat tracks are shown. For the power spectrum without the slat track several peaks are found in the range from 3-8kHz. From the source maps it was found that noise at these peaks is caused by the bracket at the suction side. When the slat tracks are installed the peaks do remain and the level changes for different slat tracks indicating that the noise is caused by the disturbed flow from the bracket interacting with the slat track downstream.

Figure 15 shows that the levels are significantly higher than for slat track 2 where no leading edge opening was present. This is in line with previous studies where it was concluded that the leading edge opening has a large influence on the measurements. The effect of the panel door is also shown especially around 18kHz. The panel decreases the sound levels by about 5dB.

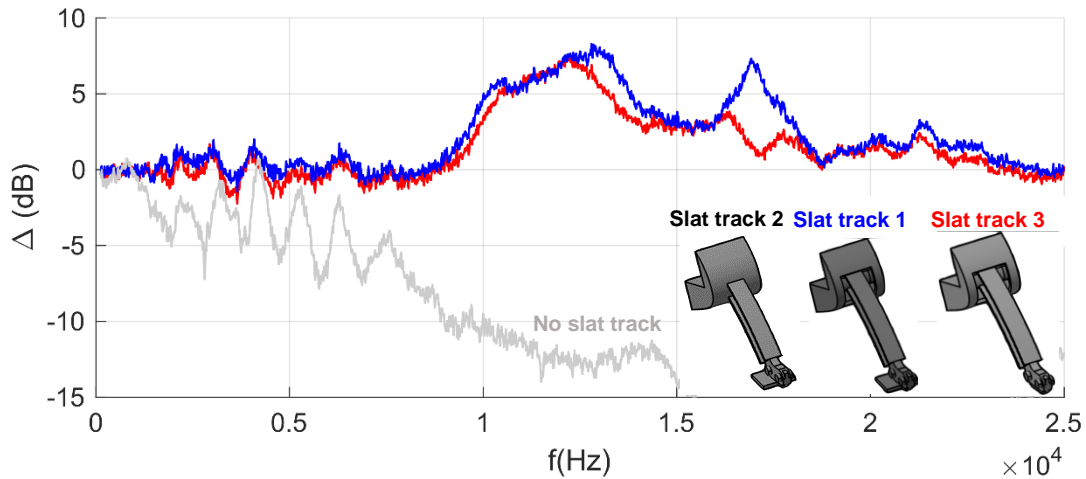


Figure 15: Power integrated spectra of baseline slat tracks. Values are relative to the power integrated spectrum of slat track 2.

In Figure 16 the slat tracks with fairings are compared to understand the influence of the slat track cross section on the noise levels. The upstream fairing from slat track 6 almost do not have an influence on the noise level. This would also be expected since separation is not avoided with this lay-out. The downstream fairing causes the noise to be lower compared to slat track 2 since separation is suppressed. In the frequency range from 5 to 10kHz the SPL levels are higher with fairing compared to without fairing. The exact reason for this needs to be further investigated.

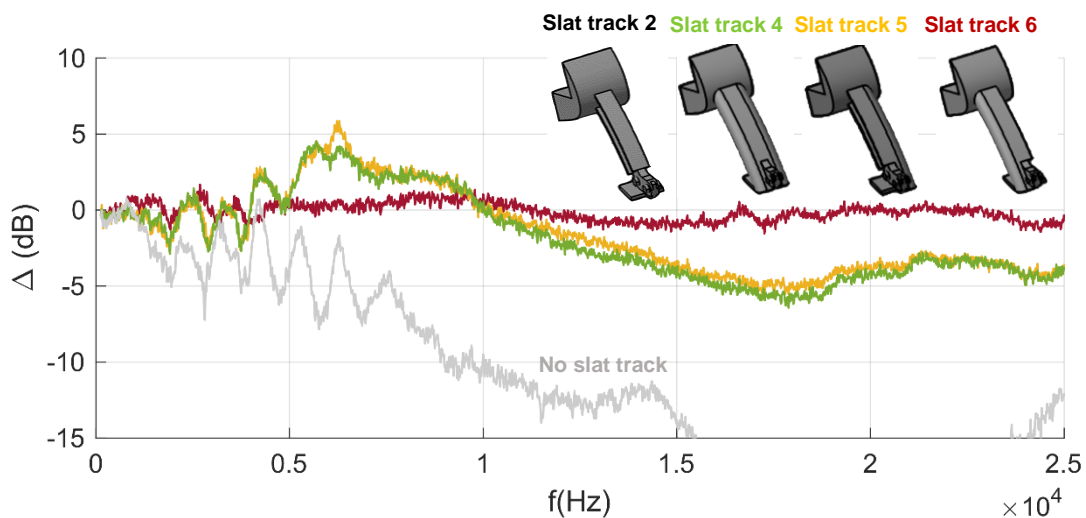


Figure 16: Power integrated spectra of slat tracks with fairing. Values are relative to the power integrated spectrum of slat track 2.

In Figure 17 the slat tracks with the tilted fairing and open configurations are compared. The tilted fairing (slat track 8) leads to a significant noise reduction from 10 to 25kHz. The open configuration by itself (slat track 9) leads to some noise reduction in the frequency range from 1 to 8kHz. When both are combined (slat track 7) it is shown that the open configuration again reduces the noise in the 1-8kHz range while at the higher frequencies it is similar to the tilted fairing alone.

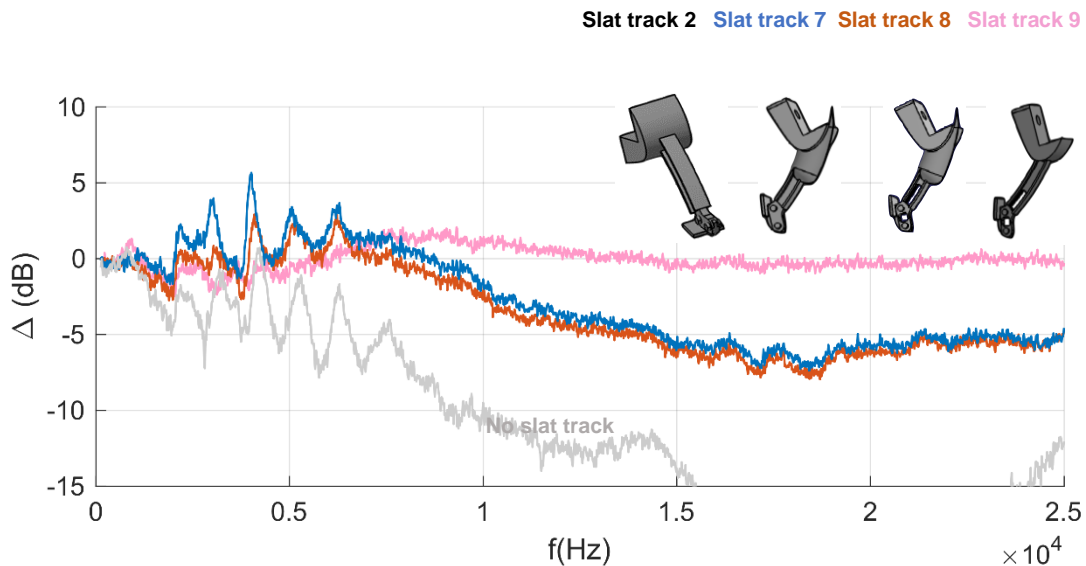


Figure 17: Power integrated spectra of slat tracks with tilted fairing and open configuration. Values are relative to the power integrated spectrum of slat track 2.

From the RANS simulations two noise generation mechanisms were identified. The noise generated by separation on the slat track at the wing side was determined to be dominating compared to the noise generated by separation on the slat track at the slat side. This is confirmed by the experimental data where the tilted fairing at the wing side leads to the largest noise reduction compared to the noise reduction by the opening at the slat side.

Finally, in Figure 18 the power spectra of the slat tracks with the lowest noise levels are compared. It is shown that the tilted fairing and opening at the slat side leads to a noise reduction of around 1-2dB compared to the fairing applied on the entire slat track.

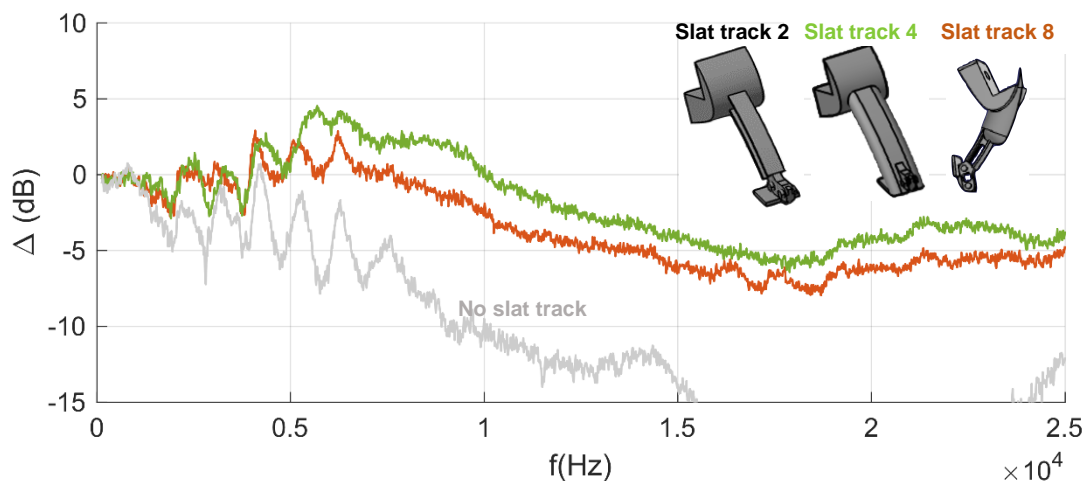


Figure 18: Power integrated spectra for slat tracks which gave the lowest noise levels. Values are relative to the power integrated spectrum of slat track 2.

4.2.3 Power integrated spectra, variations on Airbus baseline

Figure 19 shows the relative power integrated spectra for the slat track variations on the SMR commercial airliner slat track type. 'Slat track 11' was selected as reference and all levels are plotted relative to this baseline. The introduction of a slat track leads to an overall increase of noise levels of about 5dB compared to the 'no slat track' configuration. As noted above, below 7.5kHz results should be interpreted with caution due to the additional noise source related to the bracket. Nevertheless, the geometry alterations proposed for track 12 to 14 appear to have a favourable effect, showing 2-3dB reduction of noise levels. Above 7.5kHz a 2dB reduction of noise levels is found, reducing with increasing frequency until 15kHz after which no significant benefit is found.

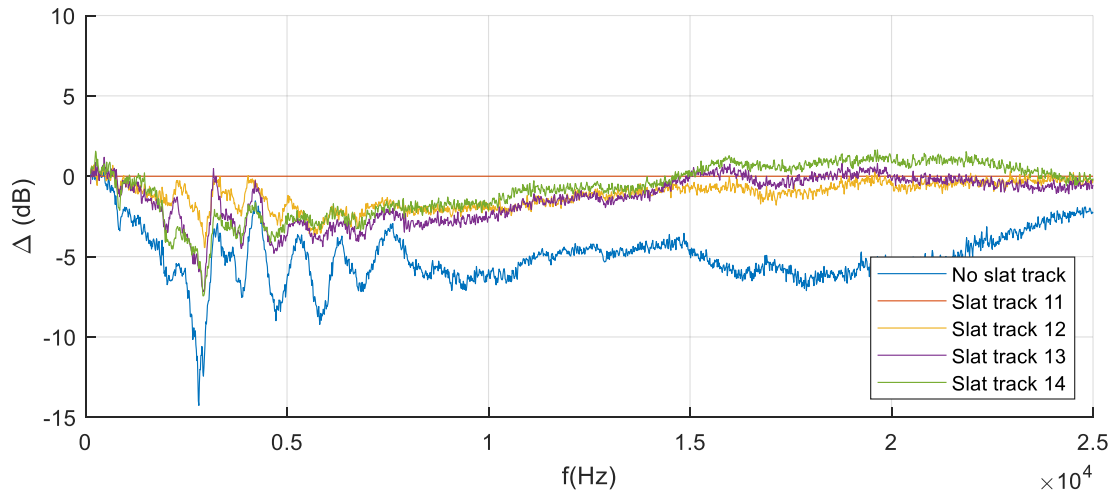


Figure 19: Power integrated spectra for DLR slat tracks.

4.2.4 Velocity scaling of noise levels

To get more insight in the noise mechanisms velocity scaling powers are derived. For the power spectrum without the slat track (not shown) several peaks are found in the range from 3-8kHz. In previous investigations on slat noise it has been shown that these peaks can be related to laminar separation on the trailing edge of the slat (Dobrzynski & Pott-Pollenske, 2001). However, from the source maps, it is found that noise at these peaks are caused by the bracket at the suction side. When the thickness of the bracket is used as length-scale L_b for the Strouhal number the peak is found around $St=0.2$ which indicates that the peaks are caused by vortices shed from the brackets. Since it can be expected that multiple sources are present at different frequency ranges, a least square fit is carried for each frequency to find n in $SPL = n \cdot 10 \log_{10}(U_\infty)$.

In Figure 20 the results for slat track 1,2 and 3 are shown. For slat track 2 the best overlap is found for $n=5.8$ up to 15kHz indicating that a dipole source is the dominating sound source. For the higher frequencies n approaches 7.5 indicating that turbulent noise described by higher order acoustic sources become more dominant. For slat track 1 and 3 the minima related to the leading opening have a lower n indicating that the flow over the leading edge cavity can be more described as a monopole type source.

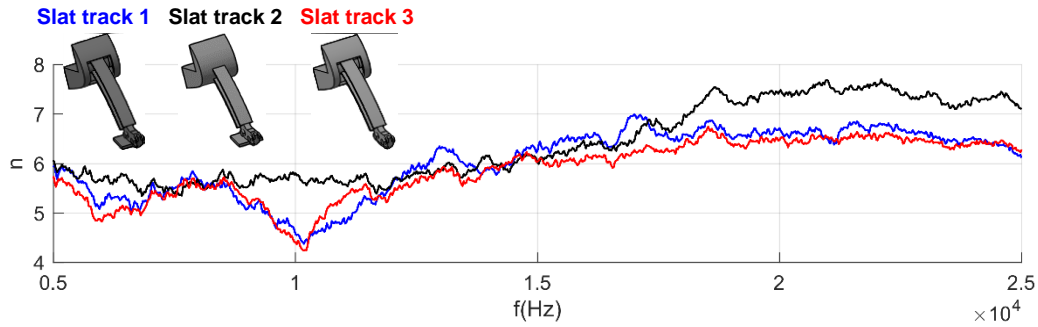


Figure 20 Slope n of the line $SPL=10n\log_{10}(U_{\infty})$ for slat track 1,2 and 3.

For slat track 4 and 5 the power integrated spectra scale best with $n=7$ up to 12kHz while for slat track 6 a similar behavior as for slat track 2 was found (Figure 21). For slat track 7,8 (Figure 22) the spectra scale well with U^6 over the entire frequency range indicating that the noise is dominated by dipole sources. Comparing to slat track 4 and 5 where $n=7$ in the high frequency range suggests that turbulent noise due to separation becomes less important due to the aerodynamically shaped fairing. For slat track 9, n is closer to 7 at the higher frequencies again indicating that higher order acoustic sources become more dominant due to the lack of fairing as was also seen for slat track 2.

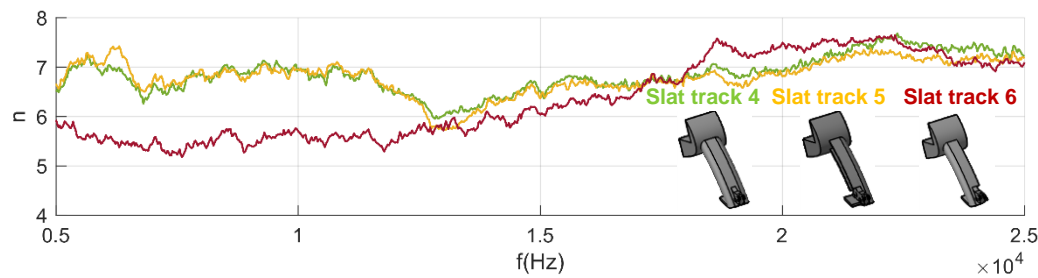


Figure 21 Slope n of the line $SPL=10n\log_{10}(U_{\infty})$ for slat track 4,5 and 6.

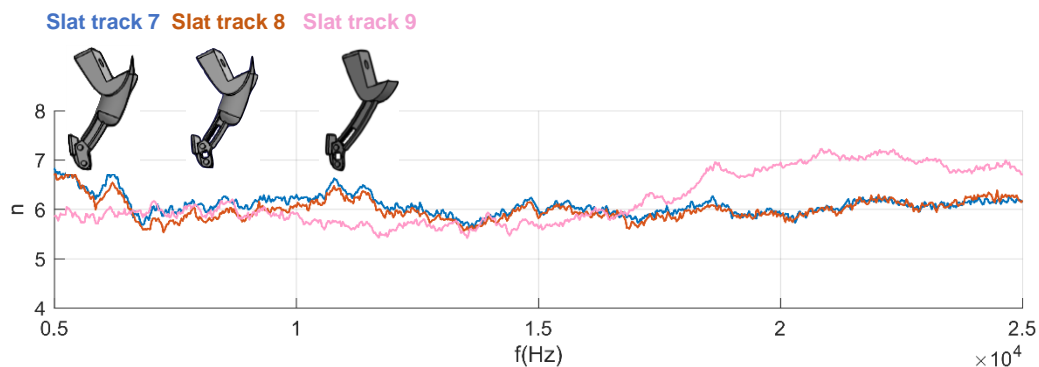


Figure 22: Slope n of the line $SPL=10n\log_{10}(U_{\infty})$ for slat track 7 to 9

5 Conclusion

In the current investigation the effect of different geometric parameters of slat tracks on slat track noise have been determined. Using insights from RANS simulations on a simplified slat track, low-noise slat tracks were designed. From the results the following conclusions can be drawn:

- As found in previous studies removing the leading edge opening leads to the largest noise reduction.
- Omitting the door panel leads to a decrease of the noise by a few dB in a narrow frequency range.
- Fairing around the slat track decreases the noise at the higher frequencies ($>10\text{kHz}$) by suppressing separation.
- A tilted fairing in combination with an opening at the slat side of the slat track decreases the noise over almost the entire frequency range.

In a further study the low-noise slat tracks will be tested in combination with other low-noise airframe components at the ONERA F2 tunnel as part of INVENTOR.

6 Bibliography

- Dobrzynski, W. et al., 2008. Research at DLR towards airframe noise prediction and reduction. *Aerospace Science and Technology*, 12(1), pp. 80-90.
- Dobrzynski, W., Nagakura, K., Gehlhar, B. & Buschbaum, A., 1998. *Airframe noise studies on wings with deployed high lift devices*. Toulouse, s.n.
- Dobrzynski, W. & Pott-Pollenske, M., 2001. *Slat noise source studies for farfield noise prediction*. s.l., s.n.
- Manoha, E., Davy, R., Pott-Polenske, M. & Barré, S., 2018. *SWAHILI: an experimental aerodynamic and acoustic database of a 2D high lift wing with sweep angle and flap side edge*. Atlanta, Georgia, AIAA.
- Murayama, M. et al., 2015. *Study on Noise Generation from Slat Tracks*. Dallas, s.n.
- Murayama, M. et al., 2016. *Study on Change of Noise Generation by Slat Track Shape*. Lyon, s.n.
- Piet, J. και συν., 2012. *Flight Test Investigation of Add-On Treatments to Reduce Aircraft Airframe Noise*. Monterey, s.n.
- Sijtsma, P. & Stoker, R., 2004. *Determination of absolute contributions of aircraft noise components using fly-over array measurements*. Manchester, s.n.
- Tuinstra, M. & van der Meulen, M., 2019. *Acoustic location by tomographic reconstruction*. Delft, 25th AIAA/CEAS Aeroacoustics Conference.
- Wang, X., Hu, Z. & Zhang, X., 2013. Aeroacoustic effects of high-lift wing slat. *International journal of aeroacoustics*, 12(3), pp. 283-307.